

Contents lists available at ScienceDirect

# Materials Letters

journal homepage: www.elsevier.com/locate/matlet





# Microstructure formation, corrosion properties, and tribological properties of laser-cladded CrCoNi medium-entropy alloy coatings

Qi Zhu<sup>a</sup>, Xueying Zhou<sup>a</sup>, Feng Yang<sup>a</sup>, Yingnan Ji<sup>a</sup>, Yan Kong<sup>a</sup>, Aiping Bi<sup>a</sup>, Zhongxiao Zhou<sup>a</sup>, Xiaomei Wang<sup>a</sup>, Ruoyu Wang<sup>b</sup>, Zhixi Zhang<sup>c</sup>, Xin Jiang<sup>a</sup>,\*

- <sup>a</sup> Central Hospital Affiliated to Shenyang Medical College, Shenyang 110032, China
- <sup>b</sup> Stomatologym Hospital of Shenyang, Shenyang 110002, China
- <sup>c</sup> Liaoning University of Traditional Chinese Medicine, Shenyang 110847, China

#### ARTICLE INFO

Keywords:
Laser cladding
Medium-entropy alloy coating
Microstructure formation
Corrosion resistance
Wear resistance

#### ABSTRACT

In this study, near-fully dense CrCoNi medium-entropy alloy coatings were deposited on an AISI 1045 steel substrate via laser cladding. Afterwards, we investigated the microstructure formation, corrosion properties, and tribological properties. Microstructural observations revealed that the CrCoNi coating has a single-phase face-centered-cubic structure and exhibits columnar grains. Furthermore, cellular substructures and elemental segregation were achieved and discussed. Potentiodynamic polarization tests in 0.1 mol/L HCl solution revealed that as compared with the AISI 1045 steel substrate, the CrCoNi coating exhibits enhanced corrosion resistance owing to a multi-stage potentiodynamic polarization behavior. Also, the dry sliding tribological tests revealed that the CrCoNi coating exhibits enhanced tribological properties due to the ultrafine microstructures and high hardness

### 1. Introduction

As novel metallic materials, high-entropy alloys (HEAs) consist of five or more elements in significant ratios [1]. HEAs exhibit excellent strength-ductility synergy [2], extraordinary corrosion resistance [3], and good tribological properties [4], etc., owing to intriguing cocktail effects, severe lattice distortion, and sluggish diffusion effects. One of the most widely investigated HEAs is the equi-atomic CrMnFeCoNi alloy with a face-centered-cubic (f.c.c.) structure [5]. Recently, the subsets of CrMnFeCoNi HEAs have received more and more attention. These subsets often consist of two to four principal elements, i.e., the so-called medium-entropy alloys (MEAs) [6]. Especially, the equiatomic CrCoNi MEA has received the most attention due to its extraordinary tensile properties and cryogenic fracture toughness [7]. Existing literature mainly used arc melting and casting to prepare bulk CrCoNi MEAs [6,8]. However, the expensiveness of constituent metals limits the industrial applications of the as-cast bulk CrCoNi MEAs. To harness the extraordinary properties and reduce the cost, some researchers have diverted to the coatings made from both HEAs and MEAs [9-10]. Laser cladding is an advanced coating fabrication technique and can rapidly fabricate coatings based on melt pool solidification [10]. We anticipate the ultrahigh cooling rates during laser cladding and the intriguing properties of HEAs and MEAs could induce high-performance coatings, owing to the strong dependency of coatings' properties on the microstructure [11–14]. In this work, CrCoNi coatings were fabricated on an AISI 1045 steel substrate by laser cladding, and the microstructure formation, corrosion and tribological resistance were studied.

## 2. Experimental

The CrCoNi powders, with a diameter of 50– $120~\mu m$ , were fabricated by the plasma rotating electrode process. The laser cladding process was performed in an argon atmosphere with the following parameters: a laser power of 400~W, a laser scan speed of 10~mm/s, and a hatch spacing of  $300~\mu m$ . The substrate material for the laser-cladded CrCoNi coating was AISI 1045 steels. The phases, microstructures, and elemental partitioning of the laser-cladded CrCoNi coating were analyzed X-ray diffraction (XRD, Rigaku D/MAX-IIA), optical microscopy (OM, Leica DM2000), scanning electron microscopy (SEM, Tescan Maia3), energy dispersive spectroscopy (EDS, Oxford), and electron backscattered diffraction (EBSD, Bruker e-Flash). The corrosion properties of both the laser-cladded CrCoNi coating and the AISI 1045 steel substrate were

E-mail address: jiangxin2023@163.com (X. Jiang).

<sup>\*</sup> Corresponding author.

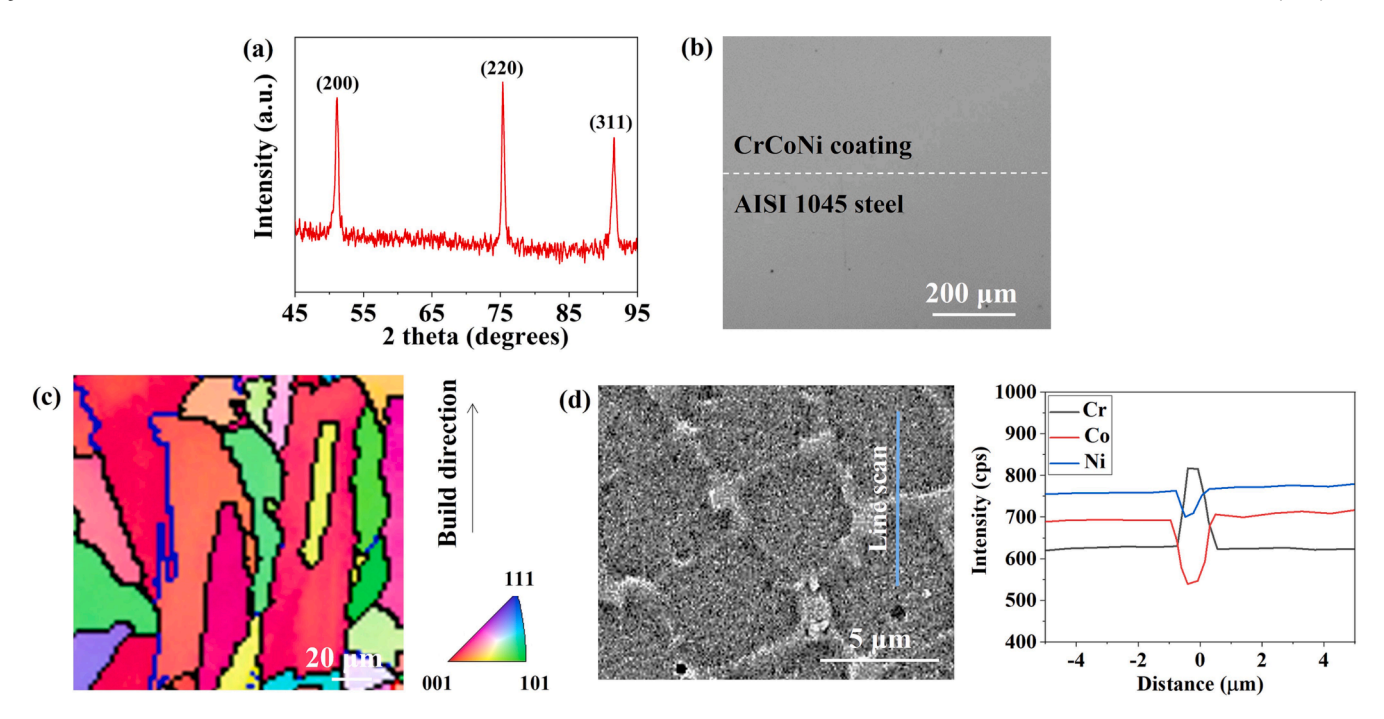


Fig. 1. (a) XRD pattern of the laser-cladded CrCoNi coating. (b) A typical OM image showing the dense CrCoNi coating and the good interfacial bonding. (c) EBSD IPF map of the as-cladded CrCoNi coating. The high angle grain boundaries (HAGBs) and low angle grain boundaries (LAGBs) are highlighted in black and blue, respectively. (d) A SEM image and corresponding EDS results showing the cellular structures and elemental partition during melt pool solidification.

tested in an acid solution of 0.1 mol/L HCl at room temperature, according to ASTM G59 standard. The three-electrode system was used, where the CrCoNi coating/the AISI 1045 steel substrate, Pt, and saturated calomel served as the working electrode, counter electrode, and reference electrode, respectively. The sample surface was polished using SiC abrasive papers, degreased with acetone and rinsed with distilled water. The effective surface had an area of 1 cm². Prior to the test, the samples were immersed for 0.5 h in 0.1 mol/L HCl acid solution to reach a steady state. The potentiodynamic polarization test was performed with a scanning rate of 0.001 V/s. The dry sliding tribological tests were performed on a HT-500 ball-on-disk tribometer with a stroke length of 16 mm, a constant load of 4 N and a frequency of 2 Hz. The Si $_3$ N4 balls with a diameter of 7.9 mm were used as the counterface materials against the laser-cladded CrCoNi coatings. The sliding duration for each individual experiment lasted for 30 min.

#### 3. Results and discussion

Fig. 1a shows the XRD profile of the laser-cladded CrCoNi MEA coating, verifying the formation of a single-phase f.c.c. structure (lattice parameter: 3.5567 Å), which is consistent with those as-cast or additively manufactured counterparts [7,15]. Fig. 1b shows a typical OM micrograph of the cross-section of the laser-cladded CrCoNi coating. Clearly, the coating well bonds with the substrate, without any visible pores and cracks at the interfacial region. The good metallurgical bonding between the coating and the substrate can be attributed to the partial remelting and the subsequent dilution of the steel substrate during laser cladding. The EBSD inverse pole figure (IPF) map in Fig. 1c clearly shows the coating has typical columnar grains which grow along the build direction, i.e., the maximum heat flux direction. As we all know, the laser cladding process establishes ultra-small melt pools and steep temperature gradients, which favor the epitaxial growth of columnar grains from layer to layer [16]. The SEM micrograph in Fig. 1d presents typical cellular substructures with distinct contrast, i.e., cellular

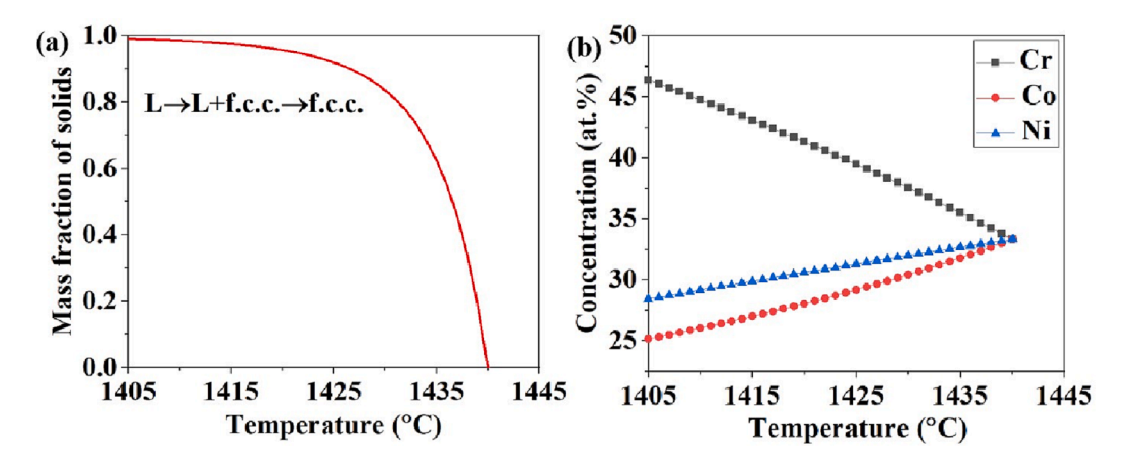
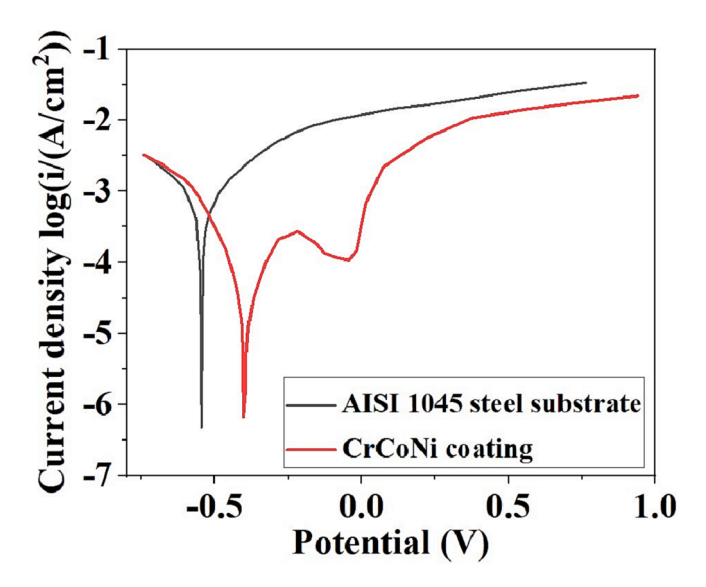
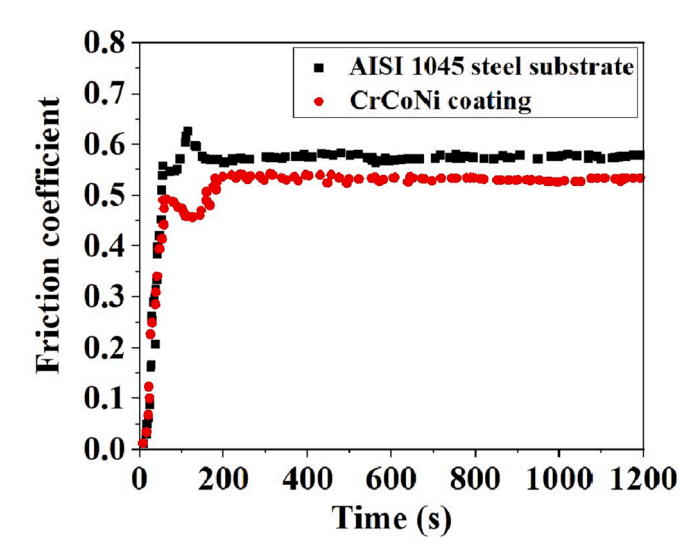


Fig. 2. Scheil simulation predicted using Thermo-Calc software as well as HEA thermodynamic database. (a) Solidification path. (b) Compositional evolution of the molten alloy with temperature.

Q. Zhu et al. Materials Letters 347 (2023) 134649



**Fig. 3.** Potentiodynamic polarization curves of the AISI 1045 steel substrate and the laser-cladded CrCoNi coating in 0.1 mol/L HCl solution.



**Fig. 4.** Friction coefficients as a function of time for both the AISI 1045 substrate and the laser-cladded CrCoNi coating.

walls and cellular interiors. The corresponding EDS analysis shows that Co, Ni elements are preferentially gathered in the region of primary solidification (i.e., cellular interior), whereas Cr elements are preferentially gathered in the region of final solidification (i.e., cellular wall). Scheil-Gulliver solidification simulation was performed to analyze the phase formation and elemental partition in the laser-cladded CrCoNi coating (Fig. 2). Specifically, we predicted a solidification path of L  $\rightarrow$  L + f.c.c.  $\rightarrow$  f.c.c., which is well consistent with our XRD pattern. Furthermore, we predicted a progressively enriched Cr elements in the remaining liquid, indicative of Cr enrichment at the cellular walls that solidify in the last stage. This is well consistent with our EDS results.

Fig. 3 shows the potentiodynamic polarization curves of the AISI 1045 steel substrate and the CrCoNi MEA coating in 0.1 mol/L HCl solution. The AISI 1045 steel substrate has a corrosion potential of  $-0.546\,$  V and a corrosion current density of 1.23E-3 A/cm². In contrast, the laser-cladded CrCoNi coating shows a higher corrosion potential of  $-0.406\,$  V and a decreased corrosion current density of 1.04E-4 A/cm², indicating an enhanced corrosion resistance. Furthermore, in contrast to the typical two-stage polarization curve (i.e., an active stage followed by a near-passive stage) of the AISI 1045 substrate, additional two stages, i.

e., the passive stage and the re-active stage, were observed for the laser-cladded CrCoNi coating. The passive potential of  $-0.217\,\mathrm{V}$  is close to the corrosion potential of  $-0.406\,\mathrm{V}$ , which facilitates the transition from the active stage to the passive stage with a small passive current density. This indicates the formation of stable passive films that can shield the sample from corrosion. Although some localized films would be broken down and exposed to the electrolyte, such damaged regions would be repaired and inhibit the intense dissolution of the coating [17]. As such, the transition from the re-active to near-passive stage would be promoted. Such multi-stage polarization behavior can delay the corrosion of the laser-cladded CrCoNi coating and hence contribute to the enhanced corrosion resistance.

The laser-cladded CrCoNi coating has a microhardness of 225 HV, which is much higher than 178 HV of the AISI 1045 steel substrate. As compared with the AISI 1045 steel substrate, the tribological properties of the laser-cladded CrCoNi coating were also enhanced. The maximum wear scar depth and width of the AISI 1045 steel substrate are 6.8 and 613 um, respectively. In contrast, the maximum wear scar depth and width of the laser-cladded CrCoNi coating decrease to 5.2 and 486 μm, respectively. The friction coefficient curves of both the AISI 1045 steel substrate and the laser-cladded CrCoNi coating are presented in Fig. 4. The average friction coefficient of the laser-cladded CrCoNi coating is 0.52, which is much smaller than that of the AISI 1045 steel substrate. The enhanced tribological properties of our laser-cladded CrCoNi coating can be attributed to the following reasons. Laser cladding is characteristic of high cooling rates up to 10<sup>3</sup>-10<sup>4</sup> °C/s, which would facilitate the formation of ultrafine microstructures, as shown in Fig. 1. Such high cooling rates-induced ultrafine microstructures and the resulting high hardness would lead to the enhanced wear resistance.

#### 4. Conclusions

In summary, we successfully fabricated CrCoNi coatings on an AISI 1045 steel substrate via laser cladding, and investigated the microstructure formation, corrosion properties, and tribological properties. The laser-cladded CrCoNi coating shows a single-phase f.c.c. structure, columnar grains, and cellular substructures. As compared with the AISI 1045 steel substrate, the laser-cladded CrCoNi coating shows a simultaneous enhancement of the corrosion and tribological resistance. The enhanced corrosion resistance of the laser-cladded CrCoNi coating has been attributed to the multi-stage potentiodynamic polarization behavior, whereas the enhanced tribological properties are attributed to the ultrafine microstructures and the high hardness.

## CRediT authorship contribution statement

Qi Zhu: Conceptualization, Methodology, Data curation, Writing – original draft, Writing – review & editing. Xueying Zhou: . Feng Yang: . Yingnan Ji: . Yan Kong: . Aiping Bi: . Zhongxiao Zhou: . Xiaomei Wang: . Ruoyu Wang: . Zhixi Zhang: . Xin Jiang: Conceptualization, Funding acquisition, Writing – review & editing.

# **Declaration of Competing Interest**

The authors declare that they have no known competing financial interests or personal relationships that could have appeared to influence the work reported in this paper.

# Data availability

Data will be made available on request.

## Acknowledgements

This study was supported by grants from the Liaoning Provincial Department of Education Basic Science Research Project (No. LJKZ1154) and also partially supported by Middle-aged and Youth Science and Technology Innovative Talents of Shenyang City (No. CR210437).

## References

- [1] J.W. Yeh, S.K. Chen, S.J. Lin, J.Y. Gan, T.S. Chin, T.T. Shun, C.H. Tsau, S.Y. Chang, Adv. Eng. Mater. 6 (5) (2004) 299–303.
- [2] P.J. Shi, W.L. Ren, T.X. Zheng, Z.M. Ren, X.L. Hou, J.C. Peng, P.F. Hu, Y.F. Gao, Y. B. Zhong, P.K. Liaw, Nat. Commun. 10 (2019).
- [3] T. Fujieda, H. Shiratori, K. Kuwabara, M. Hirota, T. Kato, K. Yamanaka, Y. Koizumi, A. Chiba, S. Watanabe, Mater. Lett. 189 (2017) 148–151.
- [4] M. Löbel, T. Lindner, T. Mehner, T. Lampke, Entropy 20 (2018).
- [5] B. Gludovatz, A. Hohenwarter, D. Catoor, E.H. Chang, E.P. George, R.O. Ritchie, Science 345 (2014) 1153–1158.
- [6] Z. Wu, H. Bei, F. Otto, G.M. Pharr, E.P. George, Intermetallics 46 (2014) 131-140.

- [7] B. Gludovatz, A. Hohenwarter, K.V.S. Thurston, H. Bei, Z. Wu, E.P. George, R. O. Ritchie, Nat. Commun. 7 (2016).
- [8] G. Laplanche, A. Kostka, C. Reinhart, J. Hunfeld, G. Eggeler, E.P. George, Acta Mater. 128 (2017) 292–303.
- [9] H. Zhang, Y. Pan, Y.Z. He, Mater. & Des. 32 (4) (2011) 1910–1915.
- [10] Y. Li, Y. Shi, Mater. Res. Express 7 (3) (2020), 036519.
- [11] M. Sabzi, S.M. Dezfuli, S.M. Far, Ceram. Int. 44 (2018) 22816–22829.
- [12] S.M. Dezfuli, M. Sabzi, Ceram. Int. 45 (2019) (1842) 21835–21842.
- [13] M. Sabzi, S.M. Dezfuli, Z. Balak, Int. J. Miner. 26 (2019) 1020-1030.
- [14] M. Sabzi, S.M. Dezfuli, S.M. Mirsaeidghazi, Ceram. Int. 44 (2018) 19492–19504.
   [15] F. Weng, Y.X. Chew, Z.G. Zhu, X.L. Yao, L.L. Wang, F.L. Ng, S.B. Liu, G.J. Bi, Addit.
- Manuf. 34 (2020), 101202. [16] Z.G. Zhu, Q.B. Nguyen, F.L. Ng, X.H. An, X.Z. Liao, P.K. Liaw, S.M.L. Nai, J. Wei,
- Scr. Mater. 154 (2018) 20–24. [17] M. Sabzi, S.M. Dezfuli, M. Asadian, A. Tafi, A. Mahaab, Mater. Res. Express 6 (2019), 076508.